

Status of Advanced Limiter-Divertor Plasma-facing Systems (ALPS) Program in the U.S.

R.F. Mattas (ANL), J.N. Brooks (ANL), J.P. Allain (UIUC), R. Bastasz (SNL), R. Doerner (UCSD), T.E. Evans (GA), A. Hassanein (ANL), T. Lutz (SNL), J. McDonald (SNL), S. Molokov (Coventry U.) R.E. Nygren (SNL), M.E. Rensink (LLNL), T. Rognlien (LLNL), D. Ruzic (UIUC), T. Tanaka (SNL), K Troncosa (SNL), M. Ulrickson (SNL), W.P. Ward (GA), W.P. West (GA), D.G. Whyte (UCSD), C.P. Wong (GA), D. Youchison (SNL)

1.0 Introduction

The Advanced Limiter-Divertor Plasma-facing Systems (ALPS) Program has been addressing issues for advanced systems since 1998 [1]. The goals of the program are:

- Establish the scientific and technological base for innovative plasma facing systems that can significantly advance fusion science and improve the vision for fusion as an energy source.
- Provide advanced plasma-facing systems and technology to the plasma physics community to enhance the performance and understanding of plasmas in existing and near term devices.

The program focus thus far has been to determine feasibility of using liquid surfaces for limiters and divertors, determine the operating windows for candidate materials, develop models to understand plasma material interactions, and conduct laboratory and tokamak tests to obtain key materials data and to determine performance. Candidate liquid surface materials include Li, SnLi, Sn, Flibe

The program is divided into four major categories.

- Plasma Edge and PMI Modeling. Modeling investigations are performed to assess the feasibility of using liquid surfaces without adversely affecting plasma performance. State-of-the-art codes are used to model the plasma edge, plasma sheath at the divertor, and particle surface interactions. The results are used to establish the operating windows for candidate liquids.
- Liquid Surface PMI Experiments. Laboratory experiments are performed to determine physical properties e.g., physical sputtering, of candidate liquids and to develop a fundamental understanding of particle interactions with liquid surfaces.
- Tokamak Experiments. Liquid lithium has been tested in CDX-U at PPPL and DIII-D at GA. The experiments have shown that lithium can safely be tested in such devices and plasma performance need not be adversely affected.
- Heat Transfer in Liquid Surfaces. Liquid surfaces potentially offer the capability to remove high heat fluxes. Flowing liquid metals in magnetically confined systems will be influenced by MHD phenomena, and work is underway to examine how MHD forces will affect heat removal capability.

Recent results in each of these areas is summarized below.

2.0 Plasma Edge and PMI Modeling

2.1 Edge-Plasma Characteristics From Transport Analysis

The properties of the plasma adjacent to divertor plates, limiters, and other plasma-facing components play a dominant role in determining the peak particle and heat fluxes incident on these surfaces. The power which drives this edge-region plasma comes from the core plasma energy input (ohmic, auxiliary, and/or alpha-particle heating). The edge plasma particle source comes from neutrals recycling from surfaces and those intentionally injected through gas puffing. We obtain the two-dimensional (2D) profiles of the edge plasma by solving a set of plasma and neutral fluid transport equations for particle continuity, parallel momentum (along the B-field), and separate ion and electron energy equations; the resulting computer code is called UEDGE [2,3]. The domain modeled includes a region a short distance inside the core boundary (defined by the magnetic separatrix) to the exterior material surfaces, and in this section, we focus on the dominant hydrogenic species in a tokamak configuration.

The output of the transport calculations give the heat load as a function of position on the material surfaces, and they also provide plasma densities and temperatures near the surfaces that are used for more detailed sheath modeling and erosion/redeposition simulations described in Sec. 2.2. The hydrogenic plasma properties also serve as the beginning state for analyzing transport of impurity and neutral particles in the edge region as discussed later. The transport models have been benchmarked extensively with present experimental data, especially from the well-diagnosed DIII-D tokamak at General Atomics, *e.g.*, Ref. 4. The primary uncertainty in the modeling is the magnitude of the turbulence-induced transport, but comparison with experiments and turbulence modeling brackets the range of values expected to be in the range of 0.1 - 4 m²/s. Two general types of divertor plasmas arise, those with high-recycling divertor plates and those with low-recycling plates, where low-recycling usually pertains to particle recycling coefficients of about 1/2 or less. High recycling gives high plasma densities at the plates and low temperatures of tens of eV or less; the detached plasma is the low temperature, recombining-plasma extreme of this regime (sometimes called a third type of divertor plasma) [5]. The low-recycling regime has low density and high temperature; this regime is less common experimentally, but if it can be produced in a reactor, may lead improved core micro-stability. However, for low recycling, a large particle flux out of the core may need to be maintained by an edge particle-fueling source such as pellets. Parameters of the regimes are illustrated in Table 1.

Table 1 Hydrogenic edge-plasma density and electron temperature at two locations for a large tokamak with low and high plate recycling coefficients.

| Hydrogen plate recycling coefficient | Midplane n_e (10^{19} m^{-3}) | Midplane T_e (eV) | Plate n_e (10^{19} m^{-3}) | Plate T_e (eV) |
|--------------------------------------|---|---------------------|--|------------------|
| $R_h = 0.25$ | 0.95 | 1090 | 0.26 | 960 |
| $R_h = 0.99$ | 3.50 | 225 | 50.9 | 76 |

2.2 Sputtering Erosion/Redeposition And Sheath Studies

The purpose of sputtering erosion/redeposition and sheath studies is to determine (1) surface temperature, plasma edge temperature, and heat flux limits on flowing liquid surface divertors, (2) impurity content in and effects on scrape off layer and edge plasma, (3) tritium codeposition in sputtered, transported, and possibly solidifying materials, (4) effects on core plasma and reactor performance, (5) compatibility between wall and divertor materials, and (6) critical data needs (e.g. self-sputtering yields).

In study [6] a sputtering erosion/redeposition analysis was performed for three candidate tokamak fusion reactor liquid divertor surfaces—lithium, tin-lithium (Sn80Li20), and flibe(LiF+BeF₂ salt). The analysis uses coupled edge-plasma, impurity-transport, and sputtering codes (UEDGE/WBC/VFTRIM), and available sputtering data. A pure lithium surface strongly absorbs impinging D-T ions—this results in a high temperature, low density, (~ 200 eV, $\sim 1 \times 10^{19}$ m⁻³) *low-recycle* plasma edge regime. Lithium appears to perform well in this regime. Although overall sputtering is high, self-sputtering is finite. Most ($\sim 95\%$) of the sputtered lithium is confined to the near-surface region and redeposited on the divertor with the remainder ($\sim 5\%$) also being redeposited after transport in the scrape-off layer. Lithium core plasma contamination is low ($\sim 10^{-4}$ Li/DT). Tin-lithium and flibe would likely operate in a high-recycle regime (e.g., 30 eV, 3×10^{20} m⁻³). Erosion/redeposition performance of these materials is also good, with finite self-sputtering and negligible core plasma contamination predicted, but with some concern about changing surface composition due to different constituent element redeposition distances. Some of the WBC/UEDGE lithium erosion/redeposition results are summarized in Figure 1 and Table 1. In spite of high redeposited Li⁺ energies and generally oblique incidence, self-sputtering is limited, comprising some 25% of the total. Of the total sputtered lithium current, $\sim 95\%$ is locally redeposited via near-surface impurity/plasma transport processes, $\sim 5\%$ leaves the near-surface region but returns to be redeposited after SOL transport, and $\sim 0.2\%$ enters the private flux region or hits the first wall. Lithium is thus mostly confined to the near surface region. A liquid surface has; of course, zero net erosion on the time scale of the liquid flow, however, gross and instantaneous (i.e., before liquid flow) net erosion rates are shown (Fig. 1) for comparison to previous solid-material studies. These rates are high, but due to the continuous replenishment, of apparently limited significance.

In summary, lithium sputtering rates are high, but the sputtered lithium is well confined close to the divertor surface with resulting low core plasma contamination. The high confinement is due to high electron-impact ionization rate coefficients, low binding energy/sputtered-velocities, and reasonably high impurity/plasma collision frequencies. Based on WBC code results for redeposited lithium ion energies and impingement angles, and on available data, we predict that lithium self-sputtering is well short of runaway. Further evaluation is needed for lower density/higher temperature plasma regimes. Other critical issues needing analysis for pure lithium are: effect of high tritium removal rates on plasma refueling requirements and helium removal by trapping in the lithium.

An important related psi/engineering issue is the maximum allowable surface temperature. The present lithium calculations are based on code/data results for 200 °C. Evaporation/sheath analysis sets an upper limit for lithium of order 500 °C [7,8]. A lower limit, however, could be set by thermally-enhanced sputtering rates as possibly seen in PISCES [9] and preliminarily in IIAX, and depending also on the spectrum (e.g. thermal) and form (atom, ion, macroscopic) of the emitted material. Figure 2 shows sputtered ion densities near the divertor surface for a tin-lithium surface. These densities are all low compared to the D-T density and fall off rapidly away from the surface. Essentially zero core plasma contamination by sputtering is predicted. For both flibe and tin-lithium the analysis shows high confinement of impurities in the near surface region with low potential for core plasma contamination, and no runaway self-sputtering. These results are encouraging but more work is needed on, for instance, full plasma profile effects, performance for different plasma edge temperatures/densities, surface temperature effects, surface segregation properties and properties of redeposited material. Sputtering data is also needed.

Table 1 summarizes various redeposition parameters for the flibe and tin-lithium components, and also as mentioned previously, for pure lithium. The sputtered tin lithium atoms have short mean free paths for ionization, due to a combination of low binding energy (lower sputtered energies), high electron density, and high ionization cross sections. Much ionization occurs in the magnetic sheath, for these high-recycling plasma conditions. Lithium from flibe behaves similarly. The beryllium and fluorine components travel longer but still fairly short distances. After ionization, subsequent strong collisional friction with the incoming plasma—and particularly for Sn and Li, sheath field acceleration—gives rise to the high local redeposition. The redeposited ion angle and energy parameters suggest data needed from sputtering experiments. For tin-lithium it is significant that redeposited Sn impacts at near-normal incidence, in contrast to the F and Be components of flibe, which redeposit at more oblique incidence.

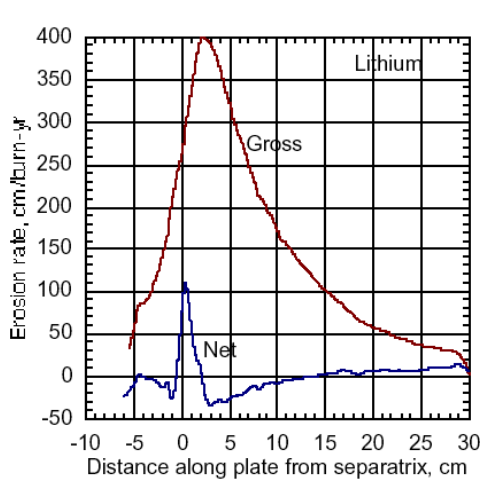


Figure 1. Gross and instantaneous (before liquid flow) net erosion rates from the WBC analysis of the lithium divertor.

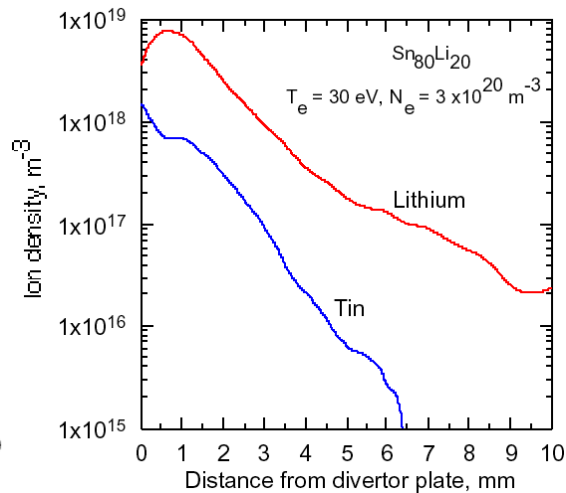


Figure 2. Sputtered ion densities near the divertor plate for a tin-lithium divertor.

Table 2. Selected erosion/redeposition parameters from WBC analysis of three liquid divertor surfaces.

| Parameter ^a | LITHIUM | TIN-LITHIUM | | FLIBE | | |
|---|---------------------------------------|-------------------|-------|-------|-------|-------|
| | (pure) | Li | Sn | Li | Be | F |
| Plasma conditions at divertor; Te(eV)/Ne(10^{20} m^{-3}) | variable; 185/0.1 at separatrix | 30/3 | | 30/3 | | |
| Binding energy, eV | 1.12 | 2.40 | 2.40 | 7.49 | 7.49 | 7.49 |
| Neutral ionization distance ^b , mm | 4.6 | 0.29 ^c | 0.15 | 0.30 | 0.86 | 1.4 |
| Charge state | 1.1 | 1.0 | 1.5 | 1.0 | 1.5 | 2.0 |
| Transit time, μs | 15 | 0.33 | 0.17 | 0.24 | 0.85 | 1.6 |
| Elevation angle, $^{\circ}$ | 53 | 32 | 15 | 30 | 42 | 42 |
| Energy, eV | 238 | 96 | 110 | 95 | 171 | 268 |
| Poloidal distance from launch point (standard deviation), mm | 70 | 2.0 | 1.1 | 1.7 | 4.7 | 7.9 |
| Redeposition fraction (for 5 cm near-surface-cutoff) | 0.950 ^d | 1.000 | 1.000 | 1.000 | 1.000 | 1.000 |

a Except where noted denotes average value for redeposited ions

b Normal to surface

c Includes effect of high reflected Li component

d Total redeposition (with SOL transport) = 0.998

In-sheath ionization of surface-emitted material can affect the tokamak type (strong Bfield at highly oblique angle) sheath. This is particularly true for a low vapor pressure material like lithium. Reference [7] describes the newly developed BPHI-3D code and initial studies for plasma sheath interactions with lithium and also for carbon. This is a Debye/magnetic tokamak-type oblique incidence magnetic field sheath, with near-surface ionization and transport of thermally emitted surface material. The analysis uses Monte Carlo, kinetic treatment for deuterium-tritium (D-T) and impurity ions/neutrals, Boltzmann/guiding-center electrons, predicted fusion edge plasma conditions for a liquid lithium divertor most evaporated lithium atoms—from a $\sim 1 \text{ cm}^2$ overheated spot—are ionized in the $\sim 1 \text{ mm}$ wide magnetic sheath. These ions are strongly redeposited due to the sheath electric field. While this redeposition minimizes core plasma contamination it increases the peak heat flux to the surface. A runaway situation is then possible due to superheating/evaporation positive feedback. Carbon may behave likewise as seen in code results obtained for a TORE SUPRA carbon limiter. A semi-analytic formula for sheath parameters as a function of emitted surface material flux was developed and verified with the code.

In study [7] the semi-analytic model is extended and the BPHI-3D code is coupled with the THERM code, which solves the non-stationary heat conduction equation also in 3D geometry. Runaway heating due to initial overheating and subsequent sheath breakdown and superheat was analyzed for lithium and carbon. For typical liquid lithium divertor conditions the critical exposure time for thermal runaway is of order 10 ms – generally greater than transient periods (e.g. ELMS) or flowing liquid exposure times. This is encouraging. Critical exposure times for carbon are much longer (~1-2s), as expected due to thermal property differences, and this may explain various “hot spot” formations in carbon systems. It is also shown that, especially for carbon materials, effects such as flake formation and deterioration of heat conductivity can play a critical role.

2.3 Hydrogen Isotope and Helium Particles Entrapment in Flowing Liquid Metals as Divertor Surfaces

The purpose of this study is to investigate ability of liquid lithium layer to absorb incoming flux of helium, deuterium and lithium. There are several implications of low recycling divertor on plasma performance. If helium particles are not entrained in the surface and pumped out of the divertor, then standard vacuum pumping techniques must be used. However, the low recycling regime also results in a low density/pressure at the pump ducts. Helium is a difficult species to vacuum pump, and it may be more difficult or impossible to get adequate pumping in this situation.

Helium ash produced from as a result of the thermonuclear reaction need to be removed at its production rate. For example, in a 2000 MW fusion power reactor with major radius = 6 m operating in the low-recycle regime, the alpha-production rate, $I_{\text{fus}} = 2000 \text{ MW} / (17.6 \text{ MeV/fusion}) = 7.1 \times 10^{20} \text{ He/s}$. The DT current, $I_{\text{DT}} = 1.6 \times 10^{23} \text{ s}^{-1}$ and for 10 % He/(D+T) fraction in core plasma, the helium current to divertor is roughly: $I_{\text{He}} = 1.6 \times 10^{22} \text{ s}^{-1}$. Helium must be removed at the production rate. Therefore, the required removal efficiency $= I_{\text{fus}} / I_{\text{He}} \approx 0.04$. Thus, we need approximately 5 % removal efficiency.

Model describing absorption of helium and DT particles by a layer of liquid metal consists of solving the diffusion equation in x-y direction as shown below in Fig. 3 with various boundary conditions. Modeling of the kinetics of particle injection, motion and interactions with the liquid lattice, and ultimate release from the surface is modeled in details using the HEIGHTS package [10]. The detail implantation of the incident Helium and Hydrogen Isotopes in liquid Li is calculated using the 3-D ITMC Monte Carlo code, part of the HEIGHTS Package [11]. The mesh size of the implantation zone can be as small as one monolayer thick to accurately predict the effect of near surface area. The particle incident energies are governed by the temperature in the SOL as well as by the sheath potential at the wall surface. The TRICS code (part of HEIGHTS) then calculate the details of Helium and Hydrogen Isotope diffusion motion, trapping (if any), and surface release in the form of molecules (D-T particles) due to the recombination mechanism [12].

Figure 4 shows He pumping coefficient as a function of Li flow velocity and He diffusion

coefficient for He particles incident energy of 1.0 keV. To achieve adequate He removal rate by the Li at diffusion coefficient $D_0 = 10^{-6} \text{ cm}^2/\text{s}$, Li velocity should be $> 20\text{-}30 \text{ m/s}$. At higher diffusion coefficients the required Li velocity is very high and can exceed 100 m/s. To achieve adequate He pumping at higher implantation energies (that can result from the low-recycle regime), reasonable Li velocities of $\approx 10 \text{ m/s}$ could be sufficient. However, if He bubbles are formed in the following Li near surface layer, significant He trapping can occur. This needs more detailed investigation.

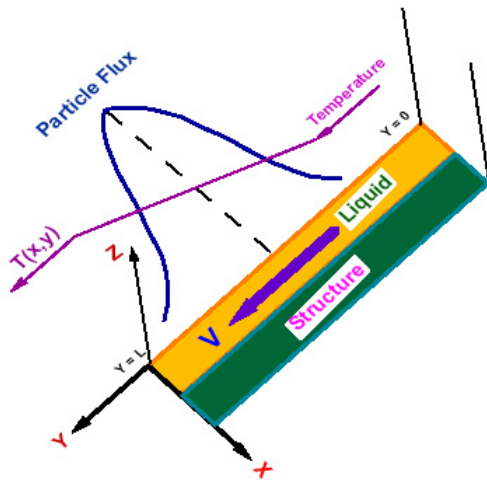


Figure 3. Schematic illustration of D/T/He interaction with liquid Surface.

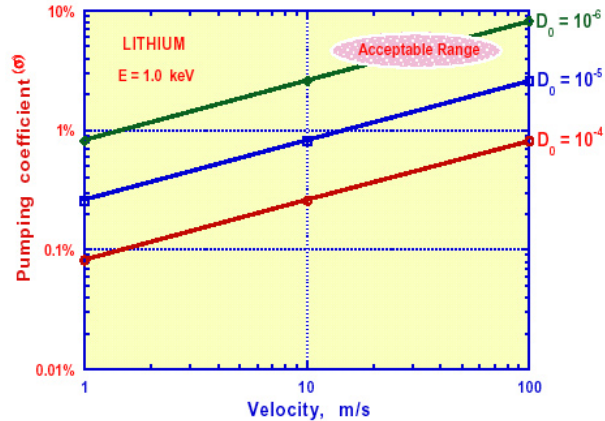


Figure 4. HEIGHTS calculations of He pumping coefficient as a function of lithium velocity

3.0 Liquid Surface PMI Experiments

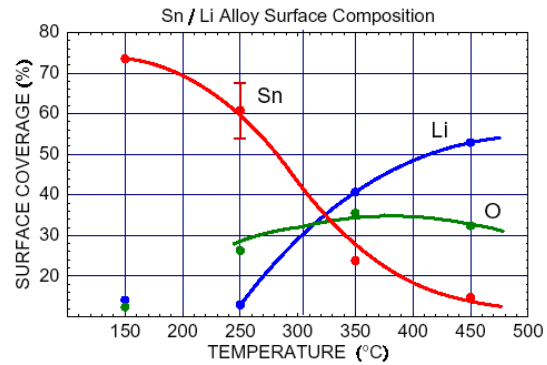
3.1 Surface Measurements of Liquid Li and Sn-Li

The composition and charge state distribution of the sputter flux originating from the divertor are important parameters for modeling erosion/deposition effects. The charged fraction of sputtered particles is immediately affected by local fields, while the neutral fraction escapes in straight-line trajectories from the surface until collisions or ionization processes occur. Furthermore, the initial velocity distribution of the sputtered particles is a function of mass. Consequently, it is necessary to obtain information about the various species sputtered from plasma-facing materials. To collect such data, a series of secondary-ion mass spectrometry (SIMS) measurements have been made of liquid Li surfaces during bombardment by hydrogen and helium ion beams. As expected, the predominant sputtered species is Li^+ . In addition, an appreciable fraction of the ionized sputter flux is comprised of Li_2 + dimers, and the oxygen-containing species Li_2O^+ and Li_3O^+ . In addition, we measured small amounts of Li_2H^+ , but little LiH^+ . We found the emission intensity of molecular Li secondary ions containing hydrogen and oxygen to be higher on the liquid surface (at 250 °C) than on the corresponding solid surface (at 25 °C).

Evidently the increased diffusivity of impurity species in the Li liquid helps to segregate hydrogen and oxygen to the liquid surface, from which they are eventually sputtered. These data provide PMI models with information about the sputter flux composition needed to better forecast erosion/deposition rates and plasma contamination levels.

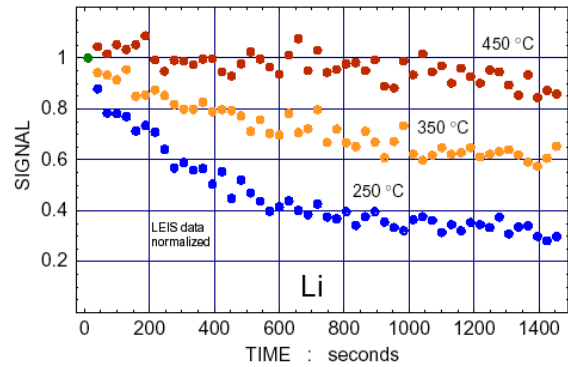
The surface composition of liquid Sn-Li was measured using low energy ion scattering (LEIS), an extremely surface-specific analysis method, as a function of temperature from below the melting point to 450 C. Upon melting, Li and O was observed to segregate to the surface, replacing Sn at the outermost atomic layer. This behavior is shown in Fig. 5. The source of the O atoms are impurities in the starting material. As the liquid temperature is raised, the O coverage begins to decrease. At operating temperatures above 410 °C, the liquid surface is predominantly Li. This observation indicates that initial surface presented to the plasma in a flowing Sn-Li alloy system will be significantly different than the bulk alloy composition. Consequently, using a Sn-Li alloy or adding Li to Sn may be beneficial by making the plasma-facing surface enriched in Li, thereby reducing the Sn sputter flux.

Figure 5. Surface composition of Sn (0.8)-Li (0.2) alloy as a function of temperature as determined by LEIS measurements. Above the melting temperature (222 °C), oxygen and lithium segregate to the surface. At temperatures above 330 °C, Li is the most prevalent atom at the surface of the liquid and the majority of surface atoms above approximately 410 °C are Li. The curves are guidelines only.



A series of measurements to measure the segregation rate of Li to the surface of a liquid Sn-Li alloy (bulk composition Sn_{0.8}Li_{0.2}) using LEIS was also conducted. These measurements build upon the techniques we developed for utilizing LEIS to examine the composition of liquid metal surfaces. The particular issue we addressed was to access how fast Li diffuses to the surface of the liquid alloy, since this rate is a major factor in determining how long a flowing liquid divertor surface can be exposed to the divertor plasma in a fusion reactor. The measurements consisted of allowing a liquid Sn-Li surface to reach an equilibrium surface composition (i.e., enriched in Li) and then monitoring the composition as the surface was bombarded with ions of known energy and flux. The measurement was repeated at various liquid alloy temperatures. At lower temperatures, the surface becomes depleted in Li. At higher temperatures and Li diffusivities, the surface remains enriched in Li. This behavior is illustrated in Fig. 6, which shows the abundance of Li at the liquid surface as a function of ion dose for 1 keV He⁺ bombardment at 68 degrees incidence from the normal.

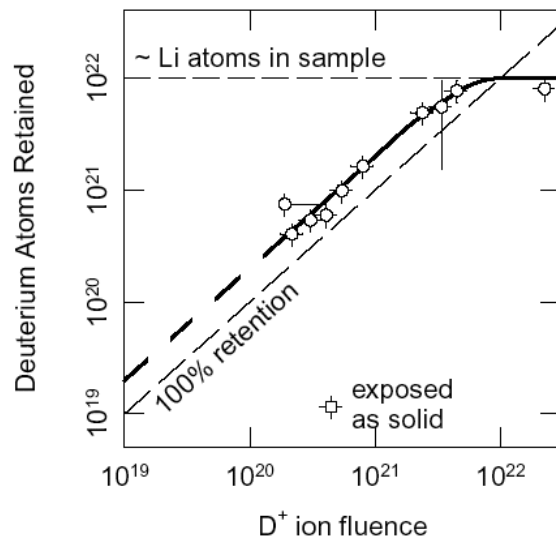
Figure 6. Time evolution of a Sn-Li liquid surface during bombardment by 1 keV He⁺ at 68° incidence from normal at a flux of about 2 · 10¹³ /cm²-s. Data are shown for three temperatures. Before beginning each measurement, the surface was allowed to equilibrate, which enriched it in Li. At 450 °C, the segregation rate of Li nearly balances its erosion rate at the surface, resulting in a nearly constant concentration of Li at the surface.



3.2 PISCES-B Experiments with Li

Much of the recent work with lithium in the PISCES Laboratory has focussed on the retention properties of lithium exposed to deuterium plasma bombardment. One of the proposed advantages of using a liquid-lithium wall in a plasma environment is its potential ability to provide a low-recycling boundary condition for a confined plasma. After developing in-situ techniques to produce pristine lithium surfaces, recent measurements now show full retention of all incident deuterium ions onto the liquid-lithium surface. In fact, the total number of deuterium atoms retained appears to be slightly larger than the integrated incident ion flux, a result that may be due to the absorption of energetic deuterium atoms incident on the lithium surface during plasma exposure. Low recycling continues until the lithium sample becomes fully hydrided (i.e. 50% Li, 50% D), at which point the retention saturates and high recycling occurs. Figure 7 shows retention data from a series of lithium samples exposed to varying fluences of deuterium plasma in PISCES-B.

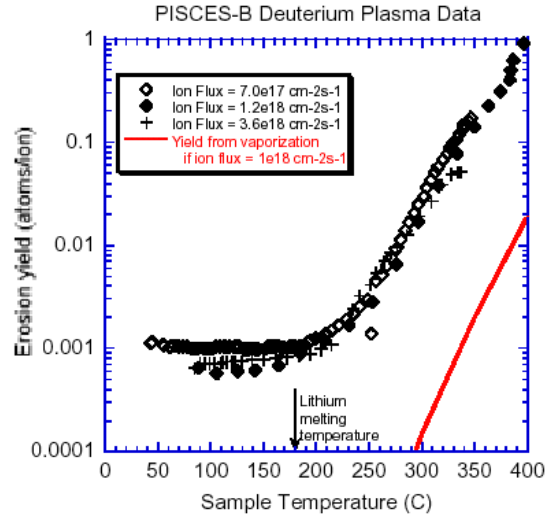
Figure 7. Deuterium atoms retained within static liquid-lithium samples (1 cm² x 0.3 cm deep) exposed to deuterium plasma bombardment in PISCES-B shows the very low deuterium recycling properties of liquid lithium. For comparison, the retention in a solid lithium sample is also shown in the figure.



Measurements continue attempting to understand the enhancement of erosion during plasma bombardment of liquid samples. Figure 8 shows the results of a flux scan on the

erosion rate of lithium samples as their temperature increases. The increase of erosion yield is seen to be independent of the incident plasma flux, indicating that the loss mechanism is tied to the incident ions. Research into possible explanations for this behavior is continuing.

Figure 8. Erosion yield of liquid lithium samples depends on the surface temperature of the sample and is independent of incident ion flux.



3.3 Experiments with Liquid Li and Sn-Li

Sputtering measurements have been taken using the Ion-surface Inter-Action Experiment (IIAX) is designed to measure the absolute, angular resolved and self-sputtering yields of many particle/target combinations [13-15]. Figure 9 shows results for Li^+ , He^+ and D^+ bombardment of liquid lithium at 45-degree incidence [14]. All sputtering yields for liquid lithium are greater than sputtering from lithium in the solid state. In both cases the relative low absolute sputtering yield of Li is directly related to the saturation of the surface by deuterium atoms. In the case of the solid phase, preferential sputtering mechanisms dominate the physical sputtering yield. In the case of lithium in the liquid phase, the relative bonding between atoms dominates the absolute sputtering of Li atoms.

Figure 9. Li^+ , He^+ and D^+ bombardment of liquid-phase lithium at 45-degree incidence measured in IIAX (Ion-surface interaction experiment). Plotted with experimental data is VFTRIM-3D simulation data.

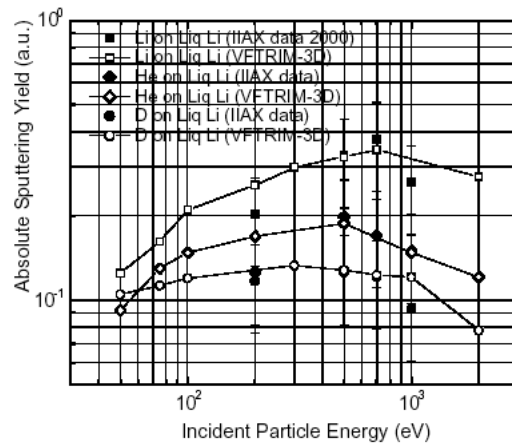
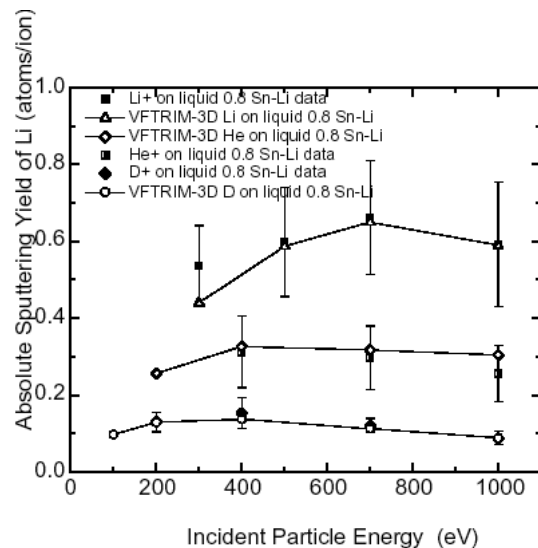


Figure 10 shows the results for Li^+ , He^+ and D^+ bombardment of liquid-phase tin-lithium

at 45-degree incidence [15]. The largest contribution to the absolute sputtering of lithium comes from bombardment by lithium ions onto liquid 0.8 Sn-Li. The maximum absolute sputtering yield of Li by Li bombardment is about a factor of two greater for helium bombardment and a factor of four greater for deuterium bombardment. This is due to a greater transfer of energy between Li bombarding ions and Li atoms on the surface, compared to D and He bombarding ions. In addition subsurface layers containing 80 a/o Sn act as a reflective wall thus leaving incident bombarding particles as highly-energetic backscattered particles, leading to more lithium sputtering. For example, incident Li atoms transfer about 16% of their energy to sub-surface Sn atoms and incident He atoms, 10%. This leaves backscattered Li and He atoms with sufficient energy to cause significant sputtering of surface Li atoms. Greater sputtering results from lithium bombardment due to their larger mass.

All sputtering yields for liquid tin-lithium are larger than those on pure lithium in liquid phase. This is primarily due to the fact that lithium is preferentially sputtered from the subsurface layers containing 80% Sn and 20% Li. In the case of pure liquid lithium, subsurface layers contribute very little lithium to the sputtering yield since in that case, deuterium is preferentially sputtered. Since solubility of deuterium in liquid tin-lithium is relatively low its contribution in decreasing the absolute sputtering yield of Li is also very low. Furthermore, the subsurface Sn-Li reflective wall as discussed above leads to greater lithium sputtering on the basis of energy transfer mechanisms. For example the maximum energy transfer factor for D atoms on Li is 0.70 compared to 0.066 for Sn.

Figure 10. Li⁺, He⁺ and D⁺ bombardment of liquid-phase tin-lithium at 45-degree incidence measured in IAX (Ion-surface interaction experiment). Plotted with experimental data is VFTRIM-3D simulation data.



4.0 Tokamak Experiments

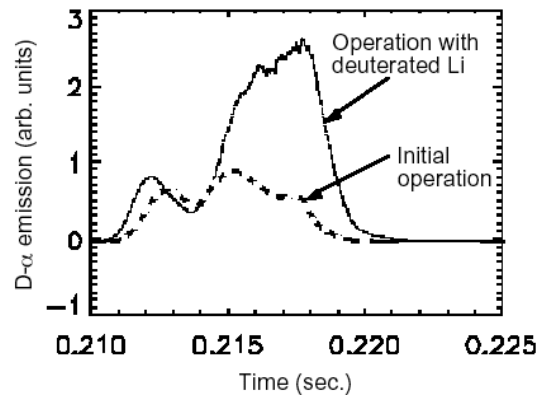
4.1 Testing in CDX-U

Significant physics and engineering problems need to be addressed before liquid metals can be considered a viable solution to the plasma wall problem. As a step toward this goal, the first experiments involving the use of solid and liquid lithium as a plasma limiter in CDX-U have recently begun, utilizing a lithium covered rail 5 cm in diameter, 20 cm long which was developed at UCSD. The lithium limiter can be inserted or

removed via a double gate valve airlock system to prevent exposure of the lithium to air. When the limiter is fully inserted, it forms the upper limiting surface for the discharge and is intended to define the last closed flux surface for the discharge. If the limiter is retracted, ceramic boron carbide rods form the upper limiting surface for the discharge. The limiter has an internal heater and has been operated in contact with the plasma over the temperature range of 20 – 260 °C.

The results of the first operation of CDX-U with a solid lithium limiter are shown in Fig. 11. Here we compare the D- α emission at the limiter surface with a lithium coating which has not been previously exposed to plasma, to the emission from a lithium coating which has been deuterated by exposure to plasma and gas puffing. Note that although recycling is markedly reduced for the case of initial operation with a solid lithium limiter, it is not eliminated. We have not yet observed any condition, for liquid or solid lithium over the ~20 - 260o C temperature range, for which recycling is completely eliminated. At this point it is unclear whether surface impurities may be responsible for the residual recycling.

Figure 11. Recycling comparison for a “fresh” lithium limiter coating (exposed to a base pressure of 3×10^{-7} T but not deuterated) and a deuterated surface. Discharge line density was identical to 5%; traces are normalized to the plasma current.



Following testing of the rail limiter, a fully toroidal limiter, consisting of a 10 cm wide tray to be filled with liquid lithium, was installed in CDX-U during the vent (Fig. 12). This will increase the lithium surface area to 1600 cm² and the in-vessel volume to approximately 0.5 liter. The boron carbide limiters on the center stack were replaced with a heat shield that was coated with titanium carbide. A heat shield was also placed below the tray, and an array of thermocouple sensors was installed around the interior of the plasma chamber. The purpose of this next step is to investigate how a large lithium surface will affect CDX-U discharges, and study the effects these plasmas will have on the magneto hydrodynamics of the liquid lithium.

For the toroidal limiter, the first experiments will be performed only with magnetic fields to determine the effect of eddy currents on the liquid lithium. The simplest measurement is to look for any motion of the lithium with a fast visible camera. The observations can then be compared with fluid MHD calculations for the CDX-U field and limiter geometry.

Figure 12. Photograph of new fully toroidal limiter tray inside CDX-U vacuum vessel.



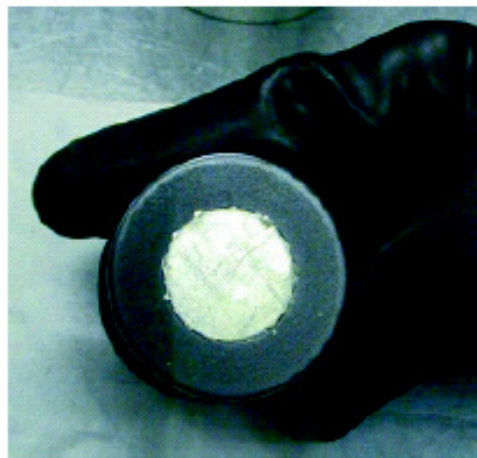
4.2 Exposure of Solid and Liquid Lithium in the DIII-D tokamak using DiMES

Lithium has been tested as a plasma-facing surface material in the divertor of the DIII-D tokamak using the DiMES sample changer system. Circular thin foils of solid lithium were conformed into a shallow 2.54 cm diameter “cup” on the DiMES sample surface (Fig. 13). Samples were not actively heated, relying instead on the incident plasma to heat and liquefy the lithium. Lithium has been exposed in the solid and liquid phase to a variety of divertor plasma conditions. These include both low power L-mode and higher power ELMing H-mode discharges. The large array of plasma and spectroscopy diagnostics on the DIII-D/ DiMES system has acquired high-quality data on the plasma-surface interaction of lithium in a tokamak divertor (Fig. 14).

Figure 13.



DiMES #106 is a graphite sample (ATJ) with a Li filled well (2.54 cm diameter, 1.3 mm deep).



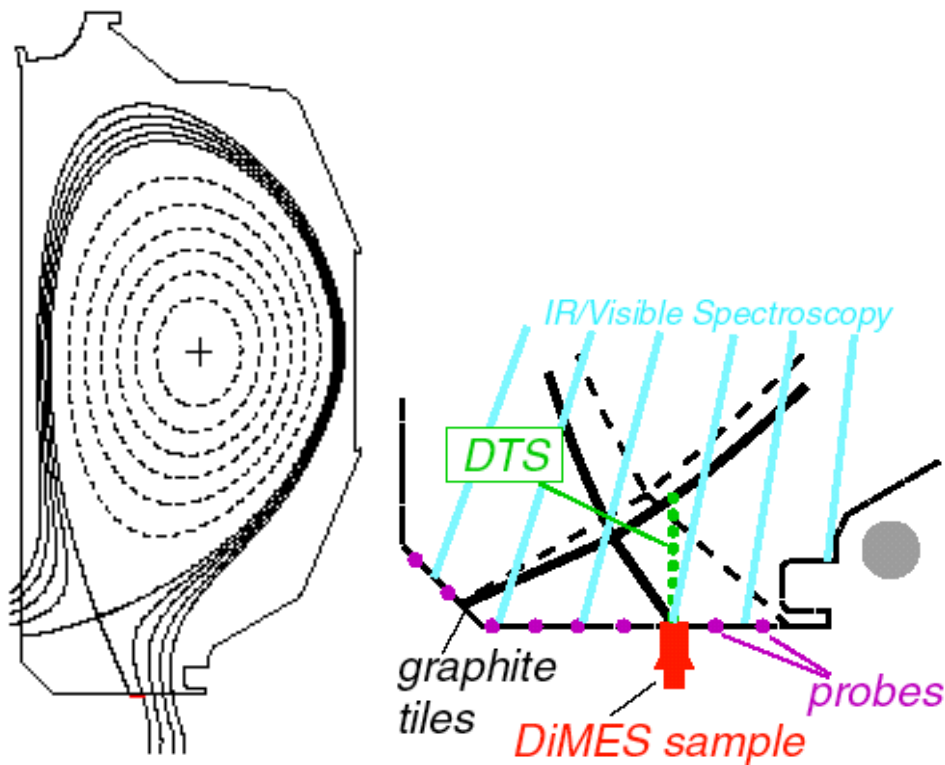


Figure 14. DiMES/DII-D provides an extensive array of plasma and Pmi diagnostics. DiMES is viewed by a visible spectrometer, three visible cameras equipped with Li filters and as an IR camera.

As a solid the effective physical sputtering yield of lithium under divertor strikepoint conditions is $<10\%$. This is significant in that the result intrinsically includes self-sputtering due to prompt lithium redeposition and the glancing angle of incidence of the magnetic field found in the divertor, both effects that enhance the total sputtering yield. The measured yield versus incident energy compares well with scaled results from laboratory measurements. Lithium yield is also in close agreement with preliminary effective yield calculations provided by J. Brooks of ANL that include self-sputtering. Therefore, it appears that lithium physical sputtering yield, which is not expected to change significantly from solid to liquid phase, is sufficiently low to be suitable for application as a plasma-facing material in the tokamak. As with the laboratory measurements, the sputtering yield is considerably less than predicted by Laszlo and Eckstein. This can be partially explained by the non-removal of ions sputtered due to the sheath; however, a full understanding of this discrepancy is not in hand. Figure 15 shows that as expected, the ionization mean-free-path for the physically sputtered lithium was found to be very small ($\ll 1$ cm) in the divertor, very effectively shielding the core plasma from the lithium erosion.

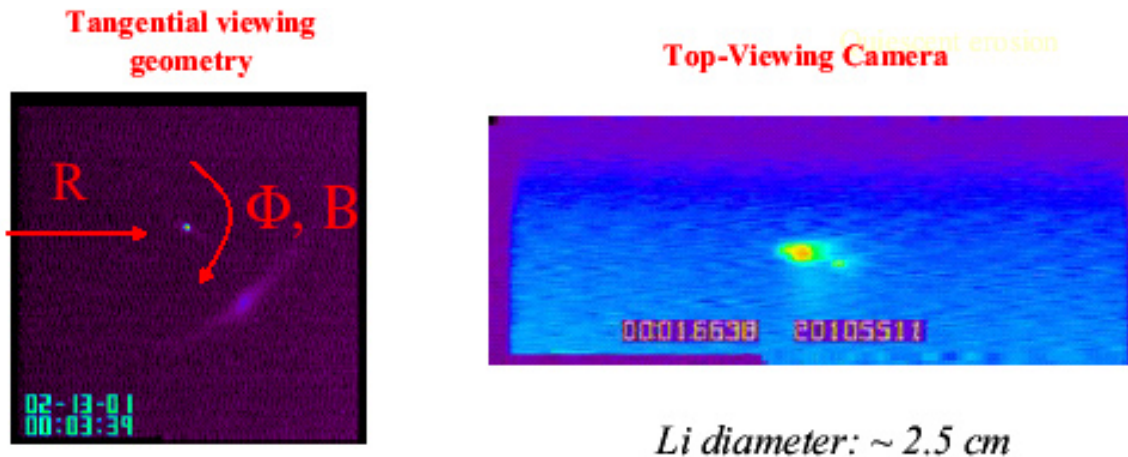


Figure 15. Imaging of Li I light during quiescent erosion of solid lithium indicates that lithium is ionized $\ll 1\text{cm}$ from target

For all DiMES exposures, including L-mode, ELMing H-mode and a discharge with a locked MHD mode, upon liquefaction, the lithium was macroscopically removed from the DiMES sample due to local $J \times B$ forces caused by the interaction of the conducting liquid and the intrinsic divertor plasma currents.

Plasma MHD events (e.g. edge localized modes, ELMs) can transiently increase SOL currents by over an order of magnitude due to the sudden release of keV particles into the SOL. For the DiMES exposures, such MHD events simultaneously provide a burst of thermal energy to liquefy the lithium sample. The result is that the $J \times B$ body forces can instantly remove the liquid lithium. This is most obvious in the case of an exposure of the lithium sample to a stationary MHD mode (locked-mode); the direction and magnitude of the measured approximately radial movement agree exactly with the expected $J \times B$ direction from locally measured vertical SOL current density in the divertor plate.

The MHD event of ELMs is also a great concern since ELMs are a product of high confinement regimes (H-Mode), presently the desirable operating regime for tokamaks. For the case of lithium exposure 5-10 cm from the strikepoint of a modest power H-mode with ELMs, it took only three ELM events to completely remove the lithium from the DiMES sample. An example of macroscopic ejection of liquid Li into the plasma is illustrated in Figure 16. This occurred during a discharge with stationary plasma conditions, the strikepoint location was fixed $\sim 3\text{ cm}$ inboard of the lithium. A large release of lithium was observed, showing near-vertical injection of lithium towards the plasma core (Fig. 16). The constant heating provided by the plasma, $q \sim 0.3\text{ MW m}^{-2}$ eventually melted the lithium.

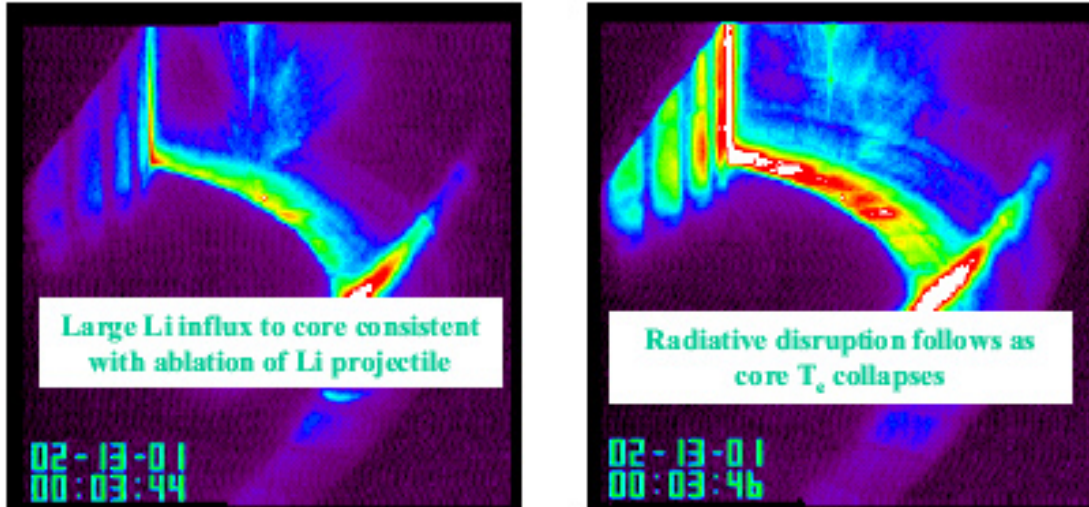


Figure 16. Video images of Li I light in divertor, following a large release of Li that causes a disruption. The likely cause of the Li influx is $J \times B$ forces, resulting in macro release of liquid Li.

5.0 Heat Transfer in Liquid Surfaces.

5.1 Modeling MHD duct flow with insulated walls

In the first part [16] of a three-part study the flow in a straight duct in a fringing magnetic field is considered. Figure 17 illustrates the configuration. The magnetic field is uniform with two different levels upstream and downstream. In the region of a nonuniform magnetic field the gradient of the field is aligned with the duct axis. The flow is assumed to be inertialess. It is analysed using an asymptotic flow model at high values of the Hartmann number, Ha . The analysis leads to two two-dimensional partial differential equations for the core pressure and the electric potential of the duct wall. These equations are solved numerically using central differences on a transformed grid. It is confirmed that for the flow in insulating circular ducts the three-dimensional effects are very significant. For fusion-reactor parameters the three-dimensional pressure drop is equivalent to the extension of the length of the duct with fully developed flow by 10-150 diameters. Finally, the effect of the finite length of the magnet in magnetohydrodynamic experiments has been evaluated.

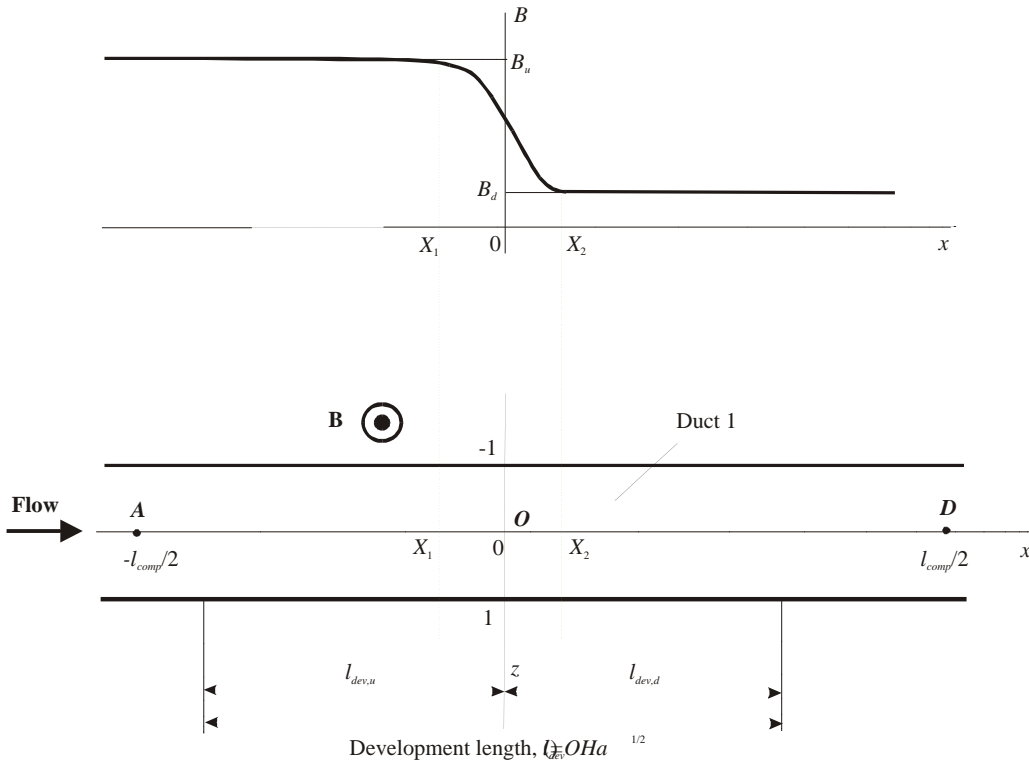
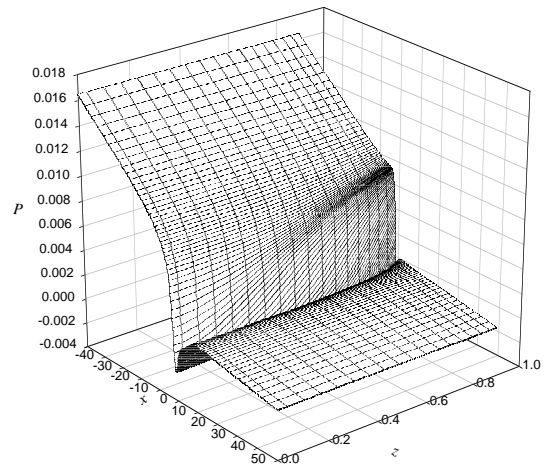


Figure 17 – Schematic diagram of the flow in a straight, circular duct: (a) non-uniform magnetic field and (b) projection of the duct in the (x,z) -plane.

As a reference case we consider the flow close to that discussed in HW89, namely $Ha = 7000$, $g = 0.8$, $B_d = 0.2$. These values are used further in all cases unless otherwise stated explicitly. For calculations in the reference case we use $l_{comp} = 100$. The results of calculations for the core pressure are shown in Figure 18.

Figure 18 – Core pressure for the reference case.

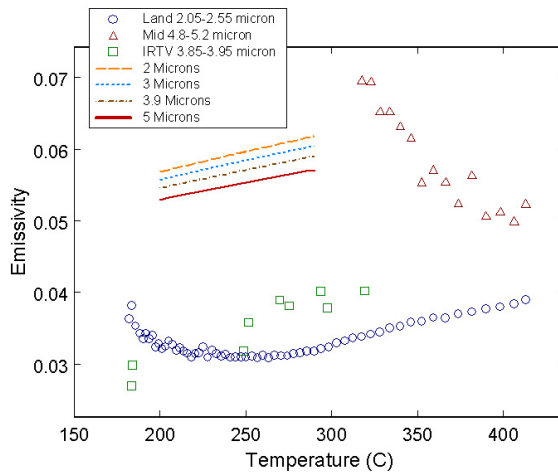


5.2 Liquid Metal IR Temperature Measurements

This section describes the tests and results of infrared temperature measurements of liquid metals performed to date. The emissivity of a material must be known to derive the temperature of a surface optically. Optical temperature measurements of the surface of a liquid metal have two major sources of error: (1) low emissive metals produce low signals that can be swamped out by reflected radiation of more emissive objects, and (2) surface contamination causes increased emissivity that can be interpreted as higher temperature. For all optical measurements of temperature, the transmission of the window and optics should be well known, because the optical losses will decrease the signal and therefore the inferred temperature. If data on emissivity are not available directly, the emissivity can be calculated from optical constants and electrical properties if these are available in the literature. In the absence of emissivity data, we have made preliminary experimental determinations and compared these with the emissivity calculated from properties in the literature. The results suggest that the calibration of our optics is still incomplete.

IR temperature measurements have been taken for Li. Lithium was the first material melted and results are shown in Fig. 19. During these measurements we found that a shorter wavelength band was useful for controlling the reflection of cool surfaces from the liquid metal surface. As a result, the IR camera is now being used with its narrow-band 3.9 μm filter.

Figure 19 – Results of emissivity measurements of liquid Li



5.3Li Loop Development

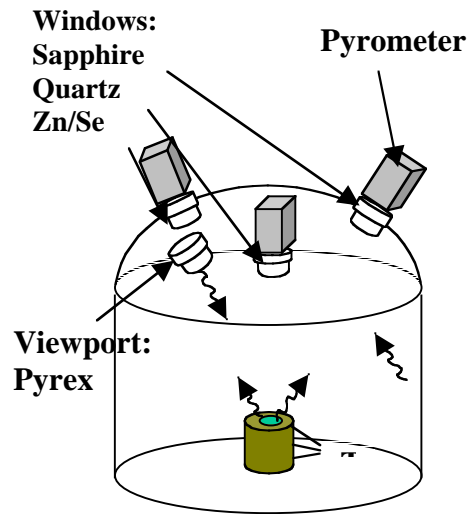
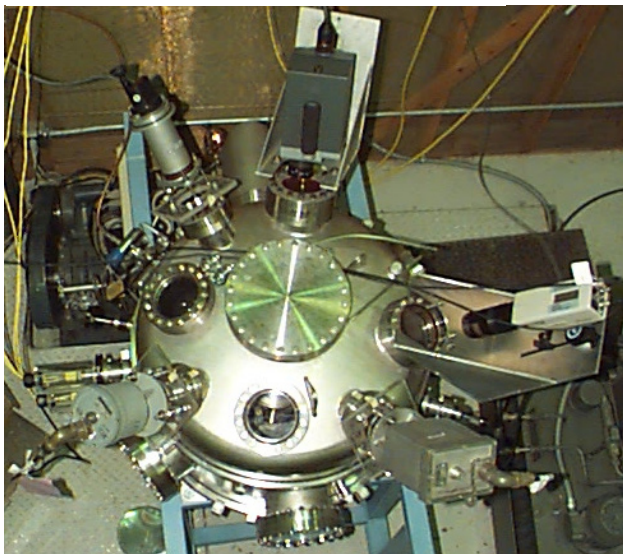
Assessing the maximum possible heat removal of a particular LS concept is a very basic objective in the development of liquid surface PFCs, and high heat flux testing is a logical approach. However, in some ways it is easier to design large (costly) HHF experiments (for example use of the ALEX loop at ANL with a neutral beam heat source)

than to design small tests. The engineering of useful small experiments that combine high heat flux with a magnetic field is by no means straightforward since an impinging heat source must be used with a free surface. One critical issue is measuring temperature distributions so that the MHD effects on heat transfer can be deduced.

Sandia has designed and will be receiving a new Li loop that will be coupled with the existing vacuum chamber now being used for our liquid metal heating tests.

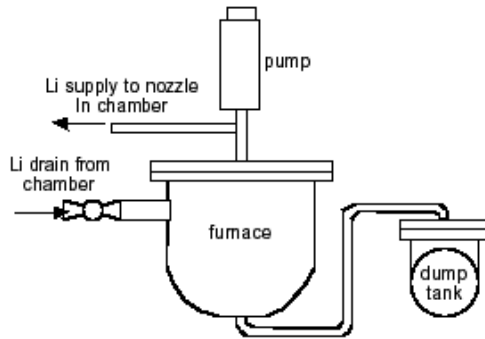
Basically the unit consists of a heated vessel, rotary pump, dump tank and associated piping and our test chamber. The heated vessel or furnace has a specified capacity of 66 liters and maximum temperature of 450°C. The specifications for the dump tank are a capacity of 82 liters and maximum temperature of 500°C. Both are made of 316L stainless steel. Figure 20 shows the test chamber; it is not yet installed into the EBTS facility and has been in use for heating tests on various liquid metals. Figure 21 is a sketch of the Li loop components. We expect to receive in August 2001 and perform initial acceptance tests. We expect the first operational test to be done with a closed pipe

Fig. 20. Liquid metal test chamber



prior to subsequent tests with free flowing Li.

Figure 21 – Sketch of Li loop components



6.0 Conclusions

- Significant progress has been made in the understanding of liquid surfaces effects in tokamaks.
- Surface temperature limits have been established for candidate liquids on the first wall and divertor.
- Several promising liquid candidates have been identified. Lithium has received the most attention.
- Laboratory experiments are providing fundamental PMI data to be used in modeling divertor and edge plasma effects.
- Tokamak experiments with Li have been performed. Experimental techniques and safety measures have been established for proper use of Li.
- Initial limiter and divertor tests with Li indicate minimal impact on plasma performance during normal operation.
- Stray currents, causing $J \times B$ forces, can lead to droplet ejection and loss of plasma control in DIII-D.
- Modeling and experimental work is in progress to address heat removal issues
- Issues to be addressed include the kinetics of particle trapping and release in liquid surfaces, MHD flow behavior of free-surfaces during normal and off-normal conditions, and influence of particle trapping

References

1. R.F. Mattas, et al., "ALPS – advanced limiter-divertor-plasma-facing systems," *Fusion Engineering and Design*, 49: 127-134, 2000
2. T.D. Rognlien, P.N. Brown, R.B. Campbell, *et al.*, *Contr. Plasma Phys.* **34**, (1994) 362.
3. T.D. Rognlien, M.E. Rensink, and G.R. Smith, "Users manual for UEDGE edgeplasma transport code," Lawrence Livermore Nat. Lab. Report UCRL-ID-127121, Jan. 21, 2000.
4. G.D. Porter, R. Isler, J. Boedo, *et al.*, *Phys. Plasmas* **7** (2000) 3663.
5. T.D. Rognlien and M.E. Rensink, "Edge-plasmas models and characteristics for magnetic fusion energy devices," submitted to *Fusion Eng. Design*, 2001.
6. J.N. Brooks, T.D. Rognlien, D.N. Ruzic, J.P. Allain, *J. Nuc. Mat.* 290-293(2001)185.
7. J.N. Brooks, D. Naujoks, *Physics of Plasmas*, 7(2000)2565.
8. D. Naujoks, J.N. Brooks, *J. Nuc. Mat.* 290-293(2001)1123.
9. R.P. Doerner et al. *ibid* p166.
10. A. Hassanein and I. Konkashbaev, "Comprehensive Physical Models and Simulation Package for Plasma/Material Interaction during Plasma Instabilities," *J. Nucl. Mater.* 273 (1999) 326.
11. A. Hassanein, "Elastic and Inelastic Surface Effects on Ion Penetration in Solids and Resulting Sputtering and Backscattering," *J. Nucl. Inst. & Method. Phys Res.* B13 (1985) 225.
12. A. Hassanein, et al, "Tritium Behavior in Eroded Dust and Debris of Plasma Facing Materials," *J. Nucl. Mater.* 258-263 (1998) 295.
13. J.P. Allain and D.N. Ruzic, *Nucl. Fusion*, submitted 2000.
14. J.P. Allain, M.R. Hendricks, D.N. Ruzic, *J. Nucl. Mater.* 290-293 (2001) 180.
15. J.P. Allain, M.R. Hendricks, D.N. Ruzic, *J. Nucl. Mater.* 290-293 (2001) 33.
16. S. Molokov, C.B. Reed, "Liquid metal flow in an insulated circular duct in a strong non-uniform magnetic field. Part 1: Straight duct and the benchmark problem", Argonne National Laboratory Report, ANL/TD/TM01-18

Argonne National Laboratory, with facilities in the states of Illinois and Idaho, is owned by the United States Government, and operated by The University of Chicago under the provisions of a contract with the Department of Energy

DISCLAIMER

This report was prepared as an account of work sponsored by an agency of the United States Government. Neither the United States Government nor any agency thereof, nor any of their employees, makes any warranty, express or implied, or assumes any legal liability or responsibility for the accuracy, completeness, or usefulness of any information, apparatus, product, or process disclosed, or represents that its use would not infringe privately owned rights. Reference herein to any specific commercial product, process, or service by trade name, trademark, manufacturer, or otherwise, does not necessarily constitute or imply its endorsement, recommendation, or favoring by the United States Government or any agency thereof. The views and opinions of authors expressed herein do not necessarily state or reflect those of the United States Government or any agency thereof.